

Interactions Between Electromagnetic and Thermal Fields in Microwave Heating of Hardened Type I-Cement Paste Using a Rectangular Waveguide (Influence of Frequency and Sample Size)

P. Rattanadecho¹
e-mail: ratphadu@engr.tu.ac.th

N. Suwannapum
W. Cha-um

Research Center of Microwave Utilization in
Engineering (RCME),
Faculty of Engineering,
Thammasat University,
Pathumthani 10120, Thailand

Microwave heating-drying of hardened Type I-cement paste using a rectangular waveguide is a relatively new area of cement-based materials research. In order to gain insight into the phenomena that occur within the waveguide together with the temperature distribution in the heated cement paste samples, a detailed knowledge of absorbed power distribution is necessary. In the present paper, a three-dimensional finite difference time domain scheme is used to determine electromagnetic fields (TE_{10} -mode) and microwave power absorbed by solving transient Maxwell's equations. Two-dimensional heat transport within the cement paste located in rectangular waveguide is used to evaluate the variations of temperature with heating time at different frequencies and sample sizes. A two-dimensional heating model is then validated against experimental results and subsequently used as a tool for efficient computational prototyping.

[DOI: 10.1115/1.2993134]

Keywords: microwave heating, rectangular waveguide, numerical, type I-cement paste, hardened

1 Introduction

In the past decade, there are many successful examples of microwave application such as the heating and drying of foods, heating and drying of ceramics, heating and drying of cement paste, and vulcanizations of rubber. A number of other analyses of the microwave heating process have appeared in the recent literature [1–11].

The microwave heating process takes place inside the material, the penetrated depth of which governs how strongly the microwaves are absorbed. It is known that the heat dissipated from the microwave energy depends on many parameters, such as the configuration and geometry of the dielectric samples, the microwave power level, the microwave field distribution, and the dielectric properties of dielectric samples.

The use of alternative techniques for heating cement paste and concrete has been investigated sporadically in the past 20 years. Two of the main forms of alternative heating are Ohmic (or direct electric) heating and microwave heating. Watson [12] reported a research on microwave heating of concrete in 1968. However, very few additional works were reported over the next 20 years. Interest in microwave heating and curing of cement-based materials was again revived in the 1980s through the present [13–21]. The use of microwave heating and drying to process concrete

potentially covers the entire spectrum of the following [12,15,19,20]:

- preheating of concretes prior to the product casting or primary curing stage
- rapid (accelerated) curing and/or drying as a primary process stage
- drying as a secondary postcuring stage

These may be required individually or in combinations that are either applied sequentially or with some overlap.

In theoretical analysis, the microwave power absorbed generally is assumed to decay exponentially into the sample following Lambert's law. However, this assumption is valid for large dimension samples where the depth of sample is much larger than the penetration depth (all microwave energy, except the reflected wave from the upper surface of the sample, is dissipated within the sample). For small samples where the depth of sample is much smaller than the penetration depth, result heat in a faster rate by microwave due to the reflection and transmission components of microwave at each interface will contribute to the resonance of standing wave configuration inside the sample, whereas resonance is completely absent for greater length scales [1]. In perspective, Lambert's exponential decay law cannot predict resonance phenomenon. Therefore, the spatial variations of the electromagnetic field within small samples must be obtained by solution of the Maxwell's equations.

The two-dimensional models of the interactions between electromagnetic field and dielectric materials have been used previously to study numerous heating processes of materials in a variety of microwave applicator configurations such as rectangular

¹Corresponding author.

Contributed by the Heat Transfer Division of ASME for publication in the JOURNAL OF HEAT TRANSFER. Manuscript received May 16, 2007; final manuscript received June 27, 2008; published online June 1, 2009. Review conducted by Cholik Chan.

Table 1 Mix proportions of cement paste used

Water-to-cement ratio (<i>w/c</i>)	Portland cement Type I (kg/m^3)	Water (kg/m^3)
0.40	1394	558

Waveguide and cavities [22,23,5–7,24]. Although most of the previous investigations considered simulations of microwave heating in solid sample, little effort has been reported on study of microwave heating of cement paste in a rectangular waveguide particularly full comparison between the mathematical simulations and experimental data. Due to the limited amount of theoretical and experimental work on microwave heating of porous media such as concrete or cement paste reported to date, the various effects are not fully understood and numbers of critical issues remain unresolved. These effects of irradiation time, working frequencies, and sample size on heating pattern have not been systematically studied.

In this work, the formulation of mathematical model for the microwave heating of hardened Type I-cement paste (henceforth "cement paste" will refer to hardened Type I-cement paste) inside a rectangular waveguide in which the microwave of TE_{10} mode operating at the specified frequencies is employed utilized three microwave frequencies of 1.5 GHz, 2.45 GHz, and 5.0 GHz in testing the model.

The mathematical models are solved numerically and compared with experimental data. In analysis, the effects of the irradiation time, working frequencies, and sample size on heating pattern are investigated in detail. The result presented here provides a basis for fundamental understanding of microwave drying of porous media such as cement paste and concrete.

2 Experimental Program

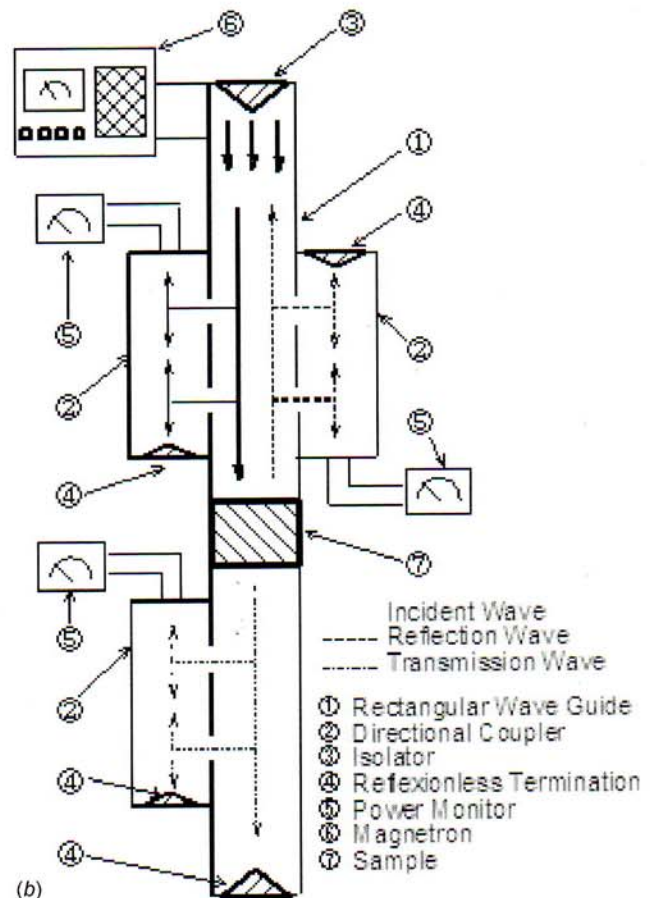
2.1 Sample Preparation. The samples studied were made with cement paste with different dimensions ($110 \text{ mm}(x) \times 54.61 \text{ mm}(y) \times 50 \text{ mm}(z)$ and $110 \text{ mm}(x) \times 54.61 \text{ mm}(y) \times 80 \text{ mm}(z)$). Portland cement type I (Blaine fineness of $3250 \text{ cm}^2/\text{g}$) is mixed with tap water ($\text{pH}=7.0$) following the ASTM C 305 Standard [25], the water-to-cement ratio (*w/c*) by weight was kept constantly equal to 0.4 in all experiments. The mixed proportions of cement paste used are shown in Table 1. After mixing and placing, the cement paste was put into mold, which was covered by plastic sheet to prevent moisture evaporation. After demolding at $23\frac{1}{2} \pm \frac{1}{2}$ h later, the samples were soaked in microwave energy.

2.2 Experimental Configuration. Figure 1(a) shows the experimental apparatus. The microwave system was a monochromatic wave of TE_{10} mode operating at a frequency of 2.45 GHz. Microwave was generated by a magnetron and transmitted along the *z*-direction of the rectangular waveguide, with an inner dimension of $110 \times 54.61 \text{ mm}^2$, toward a water load that was situated at the end of the waveguide (Fig. 1(b)). The water load (lower absorbing boundary) ensured that only a minimal amount of microwave was reflected back to the sample. The warm water load was circulated through the cooling tower to reduce the temperature in the water load system. The rectangular cement paste sample was arranged perpendicular to direction of irradiation via a rectangular waveguide. During the experiment, output of magnetron was adjusted at specified power (1000 W). The powers of incident, reflected, and transmitted waves were measured by a wattmeter using a directional coupler.

The temperature distributions within the cement paste sample were measured using fiber optic sensor (LUXTRON Fluoptic Thermometer, Model 790, accurate to $\pm 0.5^\circ\text{C}$) (measured in



(a)



(b)

Fig. 1 Schematic of experimental facility: (a) equipment setup; (b) microwave measuring system

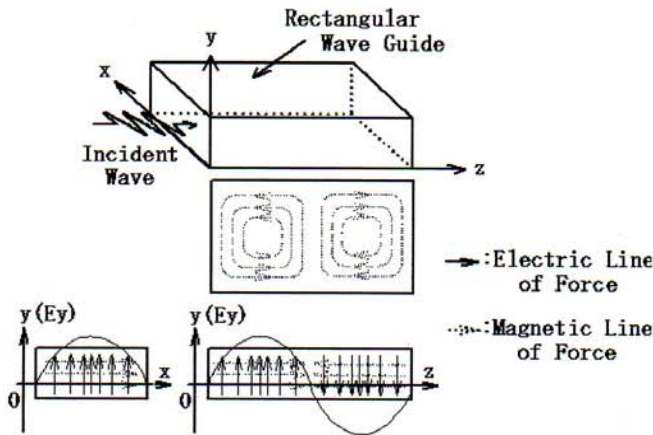


Fig. 2 Distribution of the electric field for TE₁₀ mode in a waveguide of dimensions a and b

symmetrical plane). An infrared camera was used to detect the temperature distribution at the surface of samples (x - z plane).

3 Analysis of Microwave Heating Using a Rectangular Waveguide

3.1 Physical Model. In our case, the fundamental mode, that is TE₁₀, is considered. Since microwave of TE₁₀ mode, which propagates in rectangular waveguide, is uniform in the y -direction, the three-dimensional electromagnetic field can be reduced to two-dimensional model on x - z plane (Fig. 2). Corresponding to electromagnetic field, temperature fields also can be considered in two-dimensional model. Figure 3 shows the physical model for the microwave heating of cement paste using rectangular waveguide. The model proposed is based on the following assumptions.

1. The absorption of microwave by air in rectangular waveguide is negligible.
2. The walls of rectangular waveguide are perfect conductors.
3. All materials, especially the cement paste samples, are non-magnetic.

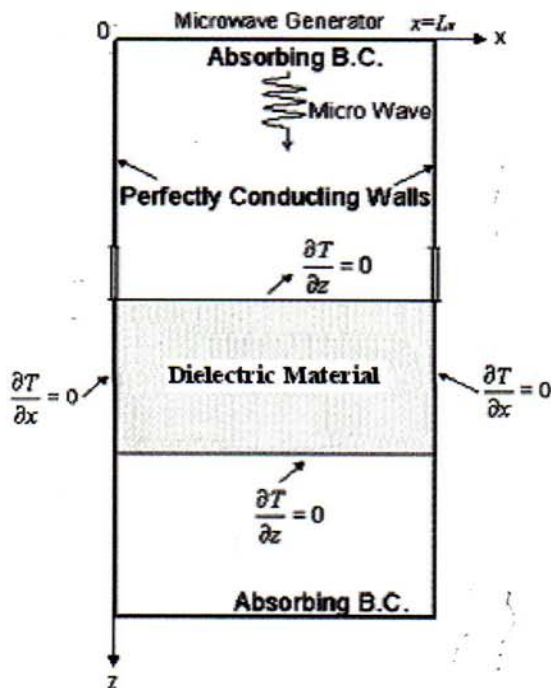


Fig. 3 Physical model

4. The effective dielectric loss factor and the effective loss tangent coefficient are assumed to vary with temperature during the heating process.
5. The effect of the sample container on the electromagnetic and temperature fields can be neglected.
6. The overall heating time is fast, and the moisture content is treated as constant throughout the numerical calculation of microwave heating process.

3.2 Maxwell's Equations. Under the assumption that microwave mode is TE₁₀, the governing equations for the electromagnetic field can be written in terms of the component notations of electric and magnetic field intensities [11]:

$$\frac{\partial E_y}{\partial z} = \mu \frac{\partial H_x}{\partial t} \quad (1)$$

$$\frac{\partial E_y}{\partial x} = -\mu \frac{\partial H_z}{\partial t} \quad (2)$$

$$-\left(\frac{\partial H_z}{\partial x} - \frac{\partial H_x}{\partial z}\right) = \sigma E_y + \varepsilon \frac{\partial E_y}{\partial t} \quad (3)$$

where E and H denote electric field intensity and magnetic field intensity, respectively. Subscripts x , y , and z represent x , y , and z components of vectors, respectively. Furthermore, permittivity or dielectric constant ε , magnetic permeability μ , and electric conductivity σ are given by

$$\varepsilon = \varepsilon_0 \varepsilon_r, \quad \mu = \mu_0, \quad \sigma = 2\pi f \varepsilon \tan \delta \quad (4)$$

In addition, if magnetic effects are negligible, which is true for most dielectric materials used in microwave heating applications, the magnetic permeability (μ) is well approximated by its value μ_0 in the free space.

Corresponding to the physical model, as shown in Fig. 3, boundary conditions can be given as follows.

- (a) *Perfectly conducting boundaries.* Boundary conditions on the inner wall surface of a rectangular waveguide are given by using Faraday's law and Gauss theorem:

$$E_t = 0, \quad H_n = 0 \quad (5)$$

- (b) *Continuity boundary condition.* Boundary conditions along the interface between different materials, for example, between air and dielectric material surfaces, are given by using Ampere's law and Gauss theorem:

$$E_t = E'_t, \quad H_t = H'_t, \quad D_n = D'_n, \quad B_n = B'_n \quad (6)$$

- (c) *Absorbing boundary condition.* At both ends of the rectangular waveguide, the first order absorbing conditions is applied:

$$\frac{\partial E_y}{\partial t} = \pm v \frac{\partial E_y}{\partial z} \quad (7)$$

Here, the symbol \pm represents forward or backward waves and v is the phase velocity of the microwave.

- (d) *Oscillation of the electric and magnetic field intensities by magnetron.* Incident wave due to magnetron is given by the following equations:

$$\begin{aligned} E_y &= E_{yin} \sin\left(\frac{\pi x}{L_x}\right) \sin(2\pi ft), \quad H_x \\ &= \frac{E_{yin}}{Z_H} \sin\left(\frac{\pi x}{L_x}\right) \sin(2\pi ft) \end{aligned} \quad (8)$$

Z_H is the wave impedance defined as

$$Z_H = \frac{\lambda_g Z_I}{\lambda_0} = \frac{\lambda_g}{\lambda_0} \sqrt{\frac{\mu_0}{\epsilon_0}} \quad (9)$$

The power flux associated with a propagating electromagnetic wave is represented by the Poynting vector:

$$S = \frac{1}{2} \text{Re}(E \times H^*) \quad (10)$$

The Poynting theorem allows the evaluation of the microwave power input. It is expressed as

$$P_{in} = \int_A S \cdot dA = \frac{A}{4Z_H} E_{yin}^2 \quad (11)$$

3.3 Heat Transport Equation. The temperature of cement paste exposed to incident wave is obtained by solving the heat transport equation with the microwave power included as a local electromagnetic heat generation term:

$$\frac{\partial T}{\partial t} = a \left(\frac{\partial^2 T}{\partial x^2} + \frac{\partial^2 T}{\partial z^2} \right) + \frac{Q}{\rho \cdot C_p} \quad (12)$$

where T is the temperature, a is the thermal diffusivity, ρ is the density, and C_p is the heat capacity at constant pressure. The local electromagnetic heat generation term Q directly depends on the electric field distribution defined as

$$Q = 2\pi \cdot f \cdot \epsilon_0 \cdot \epsilon_r (\tan \delta) E_y^2 \quad (13)$$

The initial condition of heating process is defined as $T=T_0$ at $t=0$. The boundary conditions for solving heat transport equation are shown in Fig. 3.

3.4 Dielectric Properties. In order to determine the functional temperature dependence of dielectric properties of cement paste, the theory surrounding mixing formulas is used throughout in this study. The volume fraction of water liquid and solid particle is considered as follows:

$$\epsilon_r(T) = (\epsilon'_r(T) - j\epsilon''_r(T)) \quad (14)$$

where

$$\epsilon'_r(T) = \phi \epsilon'_{ri}(T) + (1 - \phi) \epsilon'_{rp} \quad (15)$$

$$\epsilon''_r(T) = \phi \epsilon''_{ri}(T) + (1 - \phi) \epsilon''_{rp} \quad (16)$$

The effective loss tangent coefficient can be rewritten as

$$\tan \delta(T) = \frac{\epsilon''_r(T)}{\epsilon'_r(T)} \quad (17)$$

According to the above equations, the dielectric properties of liquid water are taken directly from Ref. [26] depend on temperature and those of solid particle (cement) are taken to be constant (see Table 3). According to the dielectric properties of materials, the penetration depth where the dissipated power is reduced to $1/e$ of the power entering the surface can be calculated by

$$D_p = \frac{1}{2\pi f \sqrt{\epsilon'_r \left(\sqrt{1 + \left(\frac{\epsilon''_r}{\epsilon'_r} \right)^2} - 1 \right)}} \quad (18)$$

$$= \frac{1}{2\pi f \sqrt{\epsilon'_r (\sqrt{1 + (\tan \delta)^2} - 1)}}$$

4 Numerical Technique

In order to predict the electromagnetic field, a finite difference time domain (FDTD) method is applied. In this study, the leapfrog scheme is applied to set of Maxwell's equations. The electric field

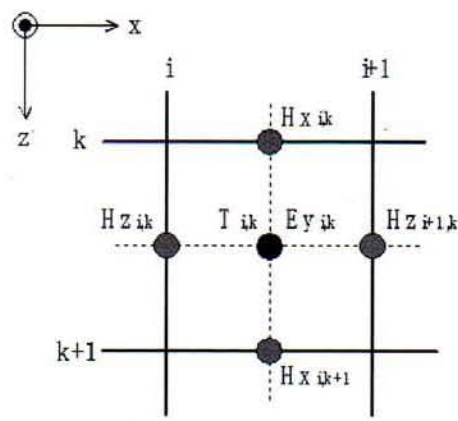


Fig. 4 Grid system configuration

vector components are offset one-half cell in the direction of their corresponding components, while the magnetic field vector components are offset one-half cell in each direction orthogonal to their corresponding components. The electric field and magnetic field are evaluated at alternative half time steps. For TE mode, the electric and magnetic field components are expressed in the total field FDTD equations as [11]

$$E_y^n(i, k) = \frac{1 - \frac{\sigma(i, k) \Delta t}{2\epsilon(i, k)}}{1 + \frac{\sigma(i, k) \Delta t}{2\epsilon(i, k)}} E_y^{n-1}(i, k) + \frac{1}{1 + \frac{\sigma(i, k) \Delta t}{2\epsilon(i, k)}} \frac{\Delta t}{\epsilon(i, k)} \times \left\{ \frac{-(H_x^{n-1/2}(i+1/2, k) - H_x^{n-1/2}(i-1/2, k))}{\Delta x} + \frac{(H_z^{n-1/2}(i, k+1/2) - H_z^{n-1/2}(i, k-1/2))}{\Delta z} \right\} \quad (19)$$

$$H_x^{n+1/2}(i, k+1/2) = H_x^{n-1/2}(i, k+1/2) + \frac{\Delta t}{\mu(i, k+1/2)} \left\{ \frac{E_y^n(i, k+1) - E_y^n(i, k)}{\Delta z} \right\} \quad (20)$$

$$H_z^{n+1/2}(i+1/2, k) = H_z^{n-1/2}(i+1/2, k) - \frac{\Delta t}{\mu(i+1/2, k)} \left\{ \frac{E_y^n(i+1, k) - E_y^n(i, k)}{\Delta x} \right\} \quad (21)$$

Furthermore, the heat transport equation (Eq. (12)) is solved by the finite difference method. The spatial and the temporal terms are approximated using finite difference equations for electromagnetic field and temperature field. Spatially, as shown in Fig. 4, Eqs. (21)–(23) and discretized heat transport equation are solved on this grid system. The choice of spatial and temporal resolutions is motivated by reasons of stability and accuracy [27–29].

To ensure stability of the time-stepping algorithm, Δt must be chosen to satisfy the Courant stability condition:

$$\Delta t \leq \frac{\sqrt{(\Delta x)^2 + (\Delta z)^2}}{v} \quad (22)$$

and the spatial resolution of each cell is defined as

$$\Delta x, \Delta z \leq \frac{\lambda_g}{10\sqrt{\epsilon_r}} \quad (23)$$

Corresponding to Eqs. (22) and (23), the calculation conditions are as follows.

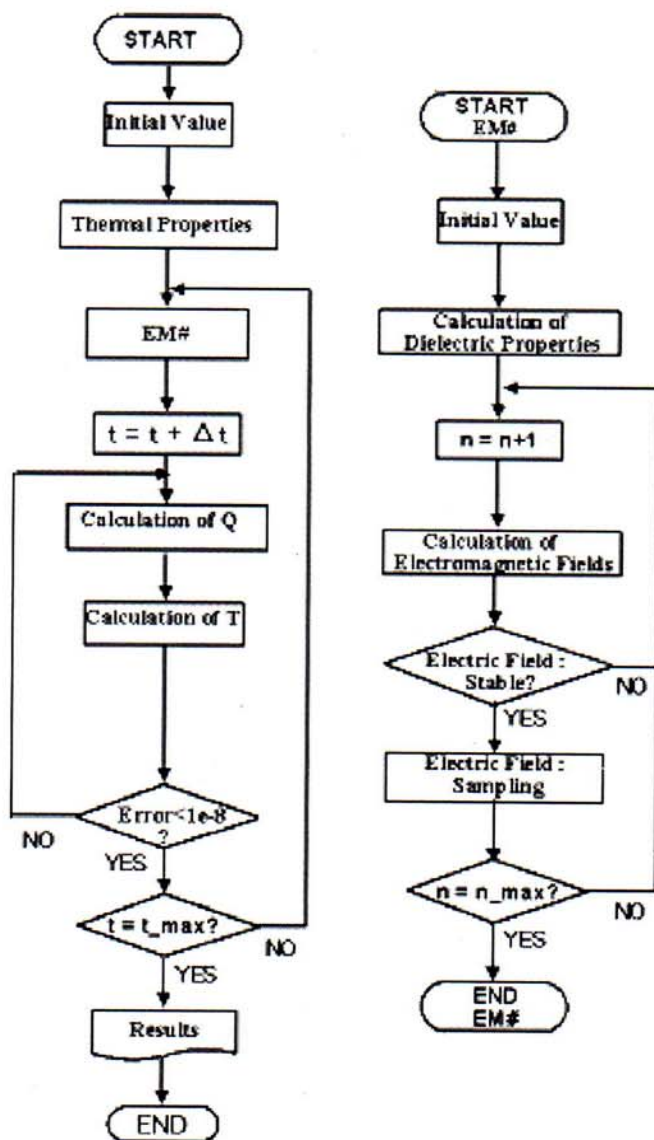


Fig. 5 Computational schemes

Table 2 Microwave power and electric field intensity relations in rectangular waveguide (1000 W)

Frequency (GHz)	Electric field intensity (V/m)
1.50	25,000
2.45	17,500
5.00	16,200

- (1) To ensure that each wavelength of the microwave in the computational domain for a frequency of 2.45 GHz has more than ten subdivisions in the numerical calculation, the computational domain is conservatively set such that the spatial resolution of each cell is $\Delta x = \Delta z \leq \lambda_{mg}/10\sqrt{\epsilon_r} \approx 1.0$ mm. Thus, the total of 110×250 cells in computational domain were used in the numerical calculation.
- (2) As the propagating velocity of microwave is very fast compared with the rate of heat transfer, the different time steps of $dt = 1$ ps and 1 s are used for the computation of the electromagnetic field and temperature field, respectively. The spatial step size is $dx = dz = 1$ mm.
- (3) The number of grid (N) is 110 (width) $\times 250$ (length).
- (4) The iteration procedure stops if relative errors are less than 10^{-8} .

5 The Iterative Computational Schemes

Since the dielectric properties of cement paste are temperature dependent, it is necessary to consider the coupling between electric field and temperature field in order to understand the influence of electromagnetic field on microwave heating realistically. For this reason, the iterative computational schemes are required to solve coupled nonlinear Maxwell's equations and heat transport equations.

The computational scheme is to first compute a local heat generation term by running an electromagnetic calculation with uniform properties, determined from initial temperature data. The electromagnetic calculation is performed until sufficient period is reached in which a representative average root-mean-square (rms) of the electric field at each spatial point is obtained, typically 30,000 time steps. The microwave power absorption at each point is computed and used to solve the time dependent temperature field. Using these temperatures, new values of the dielectric properties are calculated and used to recalculate the electromagnetic fields and microwave power absorption. All steps are repeated until the required heating time is reached. The details of computational scheme and strategy are illustrated in Fig. 5.

Table 3 Thermal properties and dielectric properties

$\epsilon_0 = 8.85419 \times 10^{-12}$ F/m	$\mu_0 = 4.0\pi \times 10^{-7}$ H/m	$\phi = 0.38$
$\epsilon_{ra} = 1.0$	$\epsilon_{rp} = 19.7$	
$\mu_{ra} = 1.0$	$\mu_{rp} = 1.0$	$\mu_{ri} = 1.0$
$\tan \delta_a = 0.0$	$\tan \delta_p = 0.29$	
$\rho_a = 1.205$ kg/m ³	$\rho_p = 2300$ kg/m ³	$\rho_i = 1000$ kg/m ³
$C_{pa} = 1.007$ kJ/kg K	$C_{pp} = 0.650$ kJ/kg K	$C_{pi} = 4.186$ kJ/kg K
$\lambda_a = 0.0262$ W/m K	$\lambda_p = 0.87$ W/m K	$\lambda_i = 0.610$ W/m K

Table 4 The ratio of penetration depth (Eq. (18)) versus sample thickness ($w/c = 0.40$)

Frequency f (GHz)	Temperature T (°C)	$\epsilon'_r(T)$	$\tan \delta(T)$	Penetration depth D_p (mm)	Penetration depth (D_p) /Sample thickness	
					$D_p/50$ mm	$D_p/80$ mm
1.50	30	35.63	0.136	51.0	1.020	0.638
	60	32.67	0.203	57.6	1.152	0.720
	90	29.97	0.195	62.7	1.254	0.784
2.45	30	35.63	0.221	31.1	0.622	0.389
	60	32.67	0.203	35.3	0.706	0.441
	90	29.97	0.195	38.4	0.768	0.481
5.00	30	35.63	0.221	15.2	0.304	0.190
	60	32.67	0.203	17.3	0.346	0.216
	90	29.97	0.195	18.8	0.376	0.234

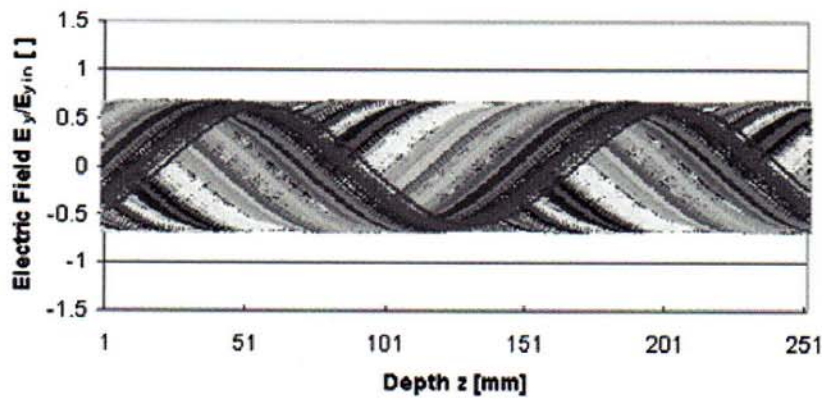


Fig. 6 The electric field distribution (Case 1)

6 Results and Discussion

In this study, the cement paste samples with a fixed water/cement ratio (w/c) of 0.4 and initial temperature of 25°C for all cases are used for analysis. Since the overall heating time is fast, the moisture content was treated as constant throughout the numerical calculation of microwave heating process. The effective dielectric loss factor and the effective loss tangent coefficient are assumed to vary with temperature during the heating process (Eqs. (14)–(17)). The output of magnetron was adjusted at specified power (1000 W) in all testing conditions. These powers can be converted into electric field intensity by using Eq. (11), as shown in Table 2. The thermal properties and dielectric properties are directly taken from Table 3. Table 4 shows the ratio of penetration depth (Eq. (18)) versus sample thickness, which can be used to provide the guidelines for discussion on the different regimes given in Figs. 11–18. In the microwave industry, only a few frequencies are available. Currently, three frequencies of 1.5 GHz, 2.45 GHz, and 5 GHz have been selected. The predicted results are then compared with experimental results for the microwave heating of cement paste. The influences of microwave frequencies and sample sizes on heating process are completely discussed in detail.

6.1 The Electric Field Distribution. To understand the electrical field distribution inside the rectangular waveguide and the cement paste sample during microwave heating, the simulation analysis is required. The simulations of the typical electric field of TE_{10} mode along the center axis ($x=54.61$ mm) of rectangular waveguide with fixed water and cement ratio (w/c) for various heating conditions are presented as follows.

- (1) Rectangular waveguide is empty; its dielectric constant is unity (which corresponds to that of air) (Case 1).
- (2) Rectangular waveguide is filled with cement paste sample operating microwave frequency of 2.45 GHz ($t=30$ s, $P=1000$ W, and size= 110 mm(x) \times 50 mm(z)) (Case 2).
- (3) Rectangular waveguide is filled with cement paste sample operating microwave frequency of 2.45 GHz ($t=30$ s, $P=1000$ W, and size= 110×80 mm²) (Case 3).
- (4) Rectangular waveguide is filled with cement paste sample operating microwave frequency of 5 GHz ($t=30$ s, $P=1000$ W, and size= 110×50 mm²) (Case 4).
- (5) Rectangular waveguide is filled with cement paste sample operating microwave frequency of 1.5 GHz ($t=30$ s, $P=1000$ W, and size= 100×50 mm²) (Case 5).

Figure 6 shows the stationary wave inside the rectangular waveguide with completely absorbed power at the end of the rectangular waveguide (Case 1). It is observed that the electric field distribution displays a wavy behavior with almost uniform amplitude along a rectangular waveguide without the sample.

Figures 7 and 8 show the electric field distribution inside a

rectangular waveguide when a sample of cement paste is inserted in the rectangular waveguide during microwave heating with a frequency of 2.45 GHz for Cases 2 and 3, respectively. Since cement paste considered as a high lossy material (as compared

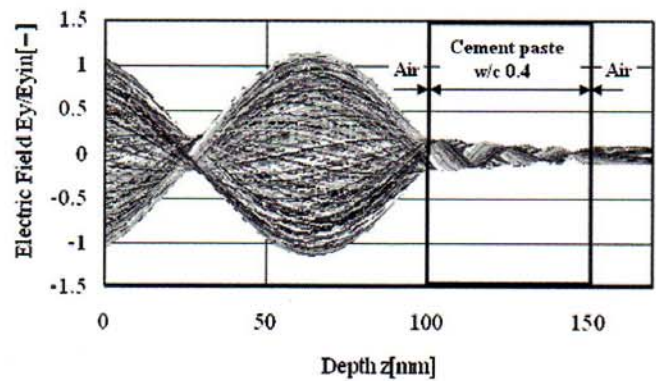


Fig. 7 The electric field distribution (Case 2)

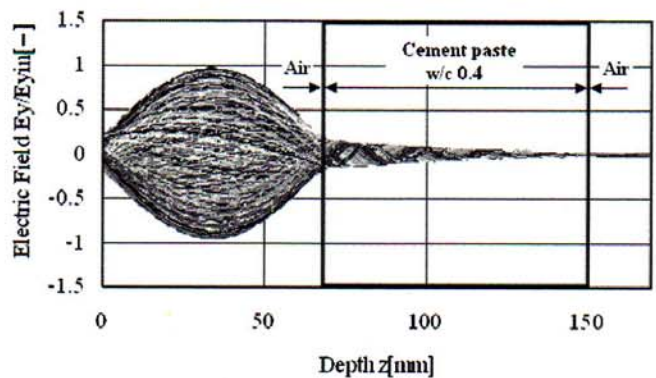


Fig. 8 The electric field distribution (Case 3)

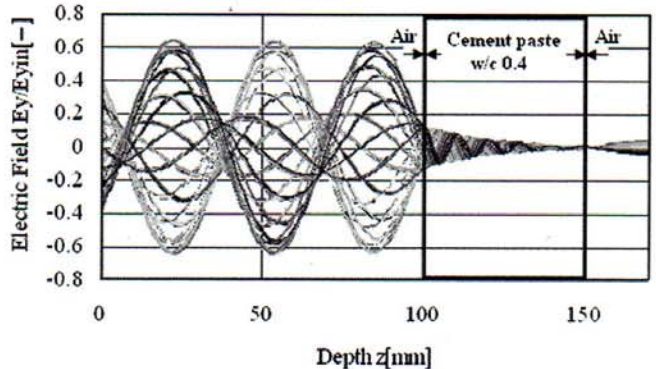


Fig. 9 The electric field distribution (Case 4)

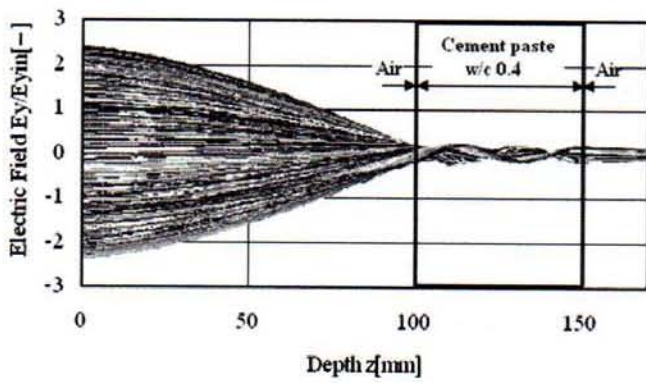


Fig. 10 The electric field distribution (Case 5)

with other materials such as wood and food stuff) has a short wavelength, which corresponds to a smaller penetration depth of microwave in comparison to the depth of sample (Table 4), larger part of microwaves is consequently absorbed by the sample. It is observed from the figures that the resonance of standing wave configuration inside the small sample (Case 2) is weak. Nevertheless, the resonance of standing wave configuration inside the large sample (Case 3) is absent due to all part of microwaves, except

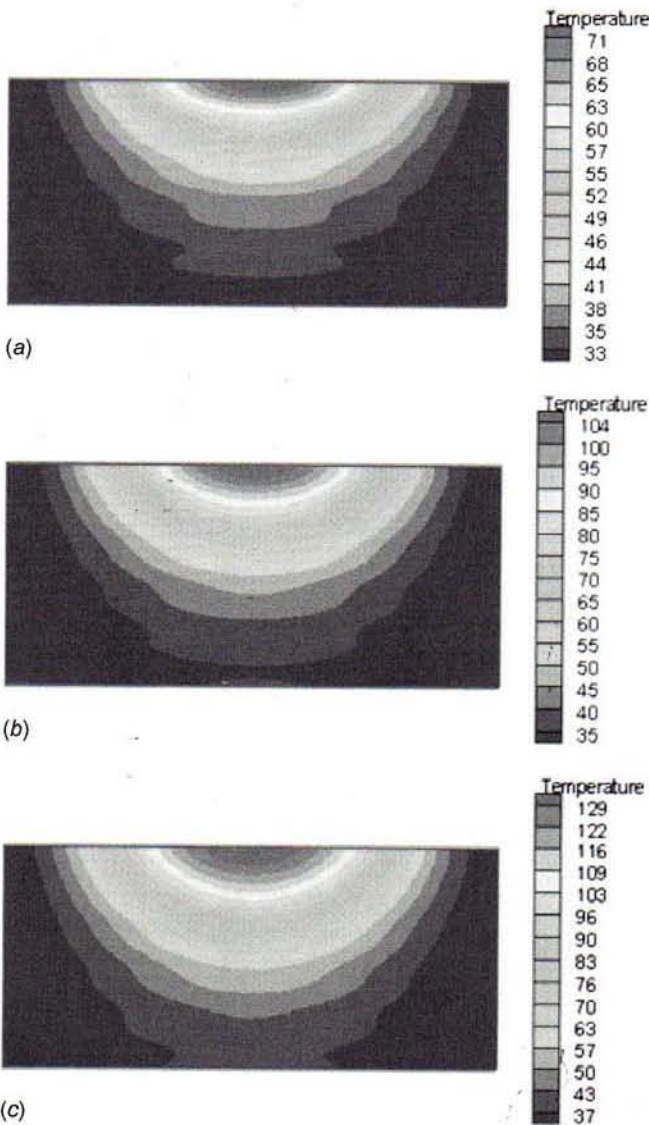


Fig. 11 Temperature distribution ($^{\circ}\text{C}$) at various heating times (Case 2): (a) 20 s; (b) 40 s; (c) 60 s

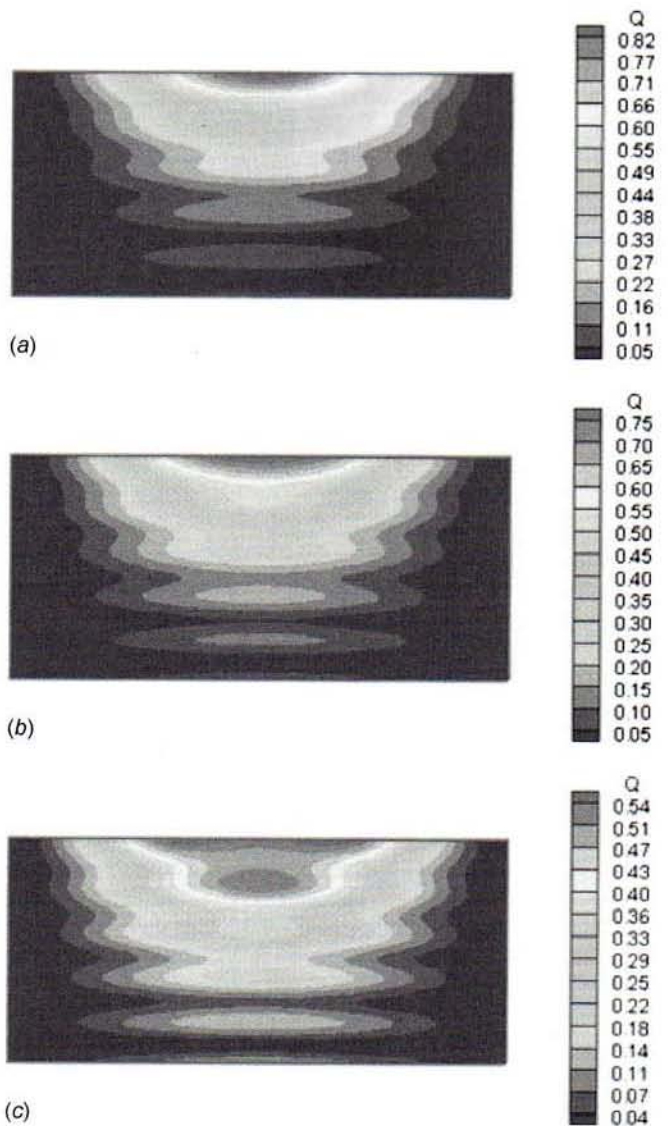
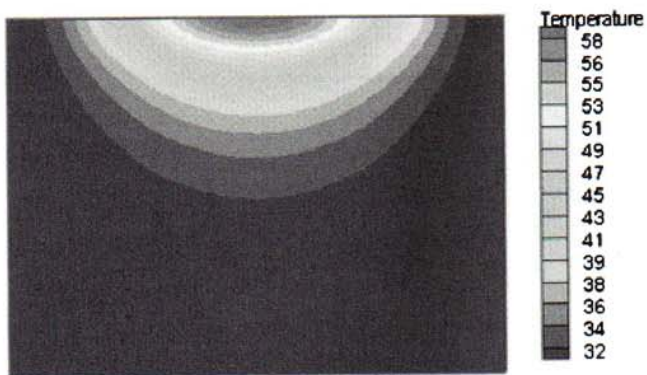


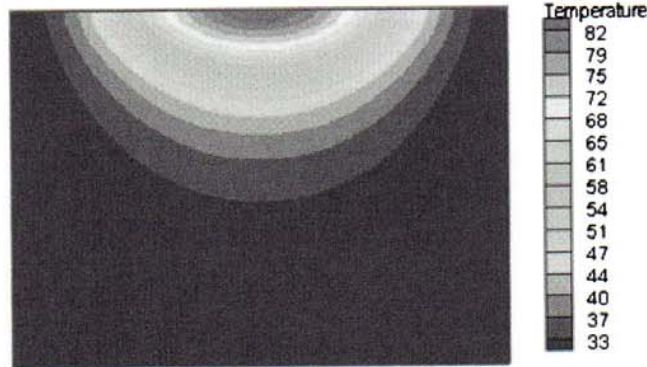
Fig. 12 Microwave power absorbed (MW/m^3) at various heating times (Case 2): (a) 20 s; (b) 40 s; (c) 60 s

the reflected wave from the upper surface of the sample that is absorbed by the sample. Focusing attention of electric field pattern inside the cavity (left hand side), a stronger standing wave with large amplitude is formed by interference between the incident and reflected waves from the surface of sample due to the different dielectric properties of materials (air and sample) at this interface. It is evident from the results that the electric field within the sample attenuates owing to energy absorption, and thereafter the absorbed energy is converted to the thermal energy, which increases the sample temperature.

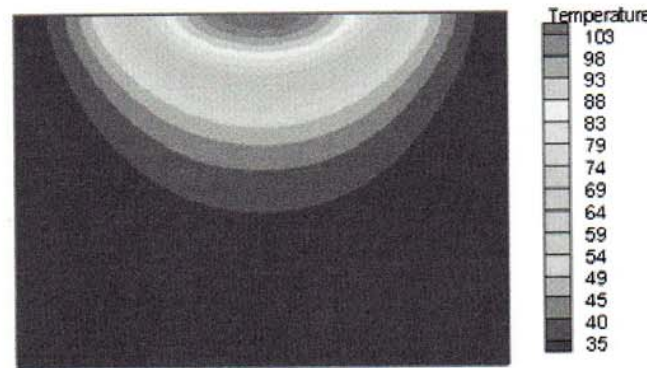
Figure 9 shows the electric field distribution when a sample of cement paste is inserted in the rectangular waveguide during microwave heating with a frequency of 5 GHz (Case 4). Since microwave operating at a high frequency has a short wavelength, which corresponds to a very small penetration depth in comparison to the depth of sample (Table 4), all microwaves, except the reflected wave from the upper surface of the sample, are consequently absorbed by the sample. It is found that the wave amplitude diminishes when z is larger the 30 mm, which results in a low microwave power absorbed. This phenomenon explains why the electric field and therefore the microwave power absorbed are the greatest at the surface exposed to incident microwaves and decay exponentially along the propagating direction with a very short wavelength. However, focusing attention of electric field



(a)



(b)



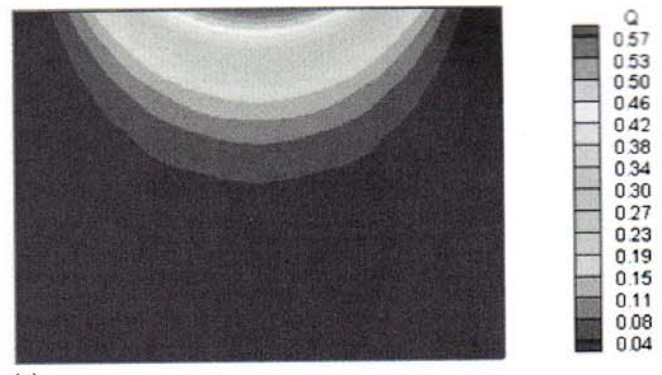
(c)

Fig. 13 Temperature distribution ($^{\circ}\text{C}$) at various heating times (Case 3): (a) 20 s; (b) 40 s, (c) 60 s

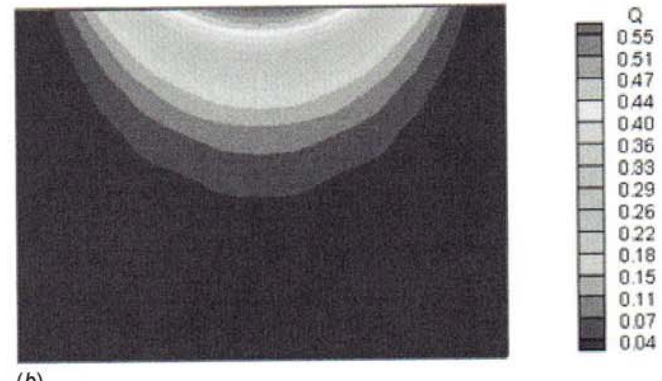
pattern inside the cavity (left hand side), a stronger standing wave with large amplitude is formed by interference between the incident and reflected waves from the surface of sample.

Figure 10 shows the electric field distribution when a sample of cement paste is inserted in the rectangular waveguide during microwave heating with a frequency of 1.5 GHz (Case 5). In this case, since microwave operating at a low frequency has a long wavelength, which corresponds to a larger penetration depth of microwave in comparison to the depth of sample (Table 4), a large part of microwaves are able to penetrate through the sample. The reflected wave will occur on each interface, air (cavity) to upper surface and lower surface of sample to air (cavity). The reflection and transmission components at each interface will contribute to the resonance of standing wave configuration inside the sample and give rise to a microwave absorption peak further from the surface exposed to incident microwaves.

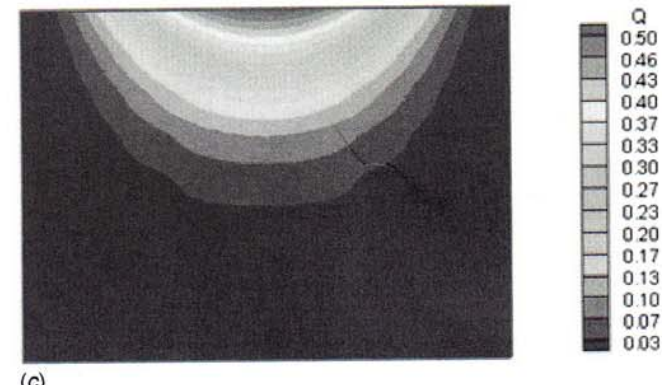
6.2 Temperature Distribution. The predictions of temperature and microwave power absorbed distributions for microwave heating of cement paste are shown in Figs. 11–20 and Fig. 22. The heating conditions correspond to Case 2, Case 3, Case 4, and Case



(a)



(b)



(c)

Fig. 14 Microwave power absorbed (MW/m^3) at various heating times (Case 3): (a) 20 s; (b) 40 s; (c) 60 s

5 as explained in the previous section.

For microwave heating of cement paste with microwave frequency of 2.45 GHz (Case 2), the predictions of temperature distribution are shown in Fig. 11. The temperature distributions correspond to the electric field distribution in the sample. This is because the electric field within the sample attenuates owing to energy absorption, and thereafter the absorbed energy is converted to the thermal energy, which increases the sample temperature. It is observed that the temperature distributions within the sample display a weak wavy behavior because the penetration depth of microwave drops dramatically and the wavelength is short. Since the reflected wave from the lower surface of the sample is almost negligible, a weak standing wave or resonance is formed within the sample. Therefore, the microwave power absorbed decreases sharply to a small value along the propagating direction (Fig. 12). Similar to the microwave power absorbed, the temperature distribution significantly varies from the maximum temperature to the minimum temperature in a short distance. The temperature distributions are shown for $t=20$ s, 40 s, and 60 s. The maximum temperature within the sample is approximately 129°C at $t=60$ s.

For microwave heating of cement paste with a large dimension

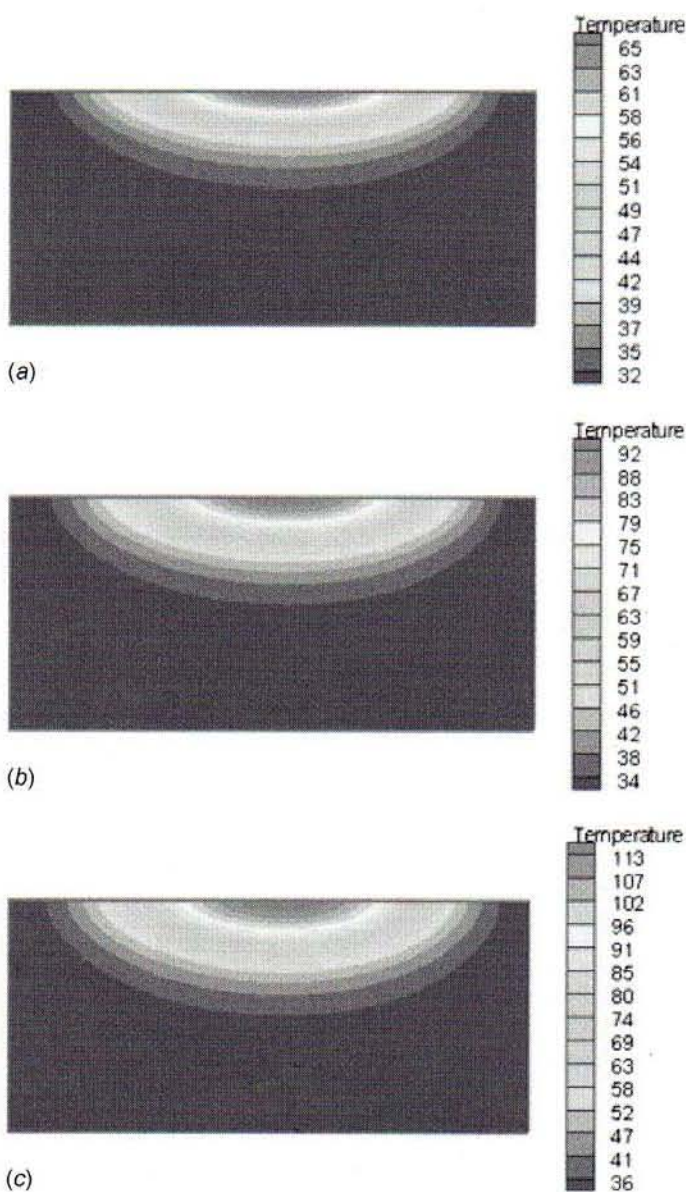


Fig. 15 Temperature distribution ($^{\circ}\text{C}$) at various heating times (Case 4): (a) 20 s; (b) 40 s; (c) 60 s

(Case 3), the predictions of temperature distribution and microwave power absorbed are shown in Figs. 13 and 14, respectively. In contrast to that case of a small sample size (Case 2), the wavy behavior within the sample is totally absent due to the negligible reflected wave from the lower surface of the sample. No standing wave or resonance is formed within the sample. This figure highlights that the larger sample has different heating characteristics in comparison with the smaller sample. The maximum power absorbed and maximum temperatures are lower as compared with Case 2 (Figs. 11 and 12). This is because the presence of the resonance has a substantial effect on the shape of the transient temperature distribution as well as microwave power absorbed. The temperature distributions are shown for $t=20$ s, 40 s, and 60 s. The maximum temperature within the sample is approximately 103°C at $t=60$ s.

For microwave heating of cement paste with microwave frequency of 5 GHz (Case 4), the predictions of temperature distributions are shown in Fig. 15. The temperature and microwave power absorbed distributions correspond to the electric field distribution in the sample (Fig. 9). It is observed that the wavy behavior of the temperature distributions within the sample is absent and it is totally different from those cases of smaller microwave frequency. This is because the reflected wave from the lower surface of the sample is negligible, and no standing wave or resonance is formed within the sample. Therefore, all microwaves,

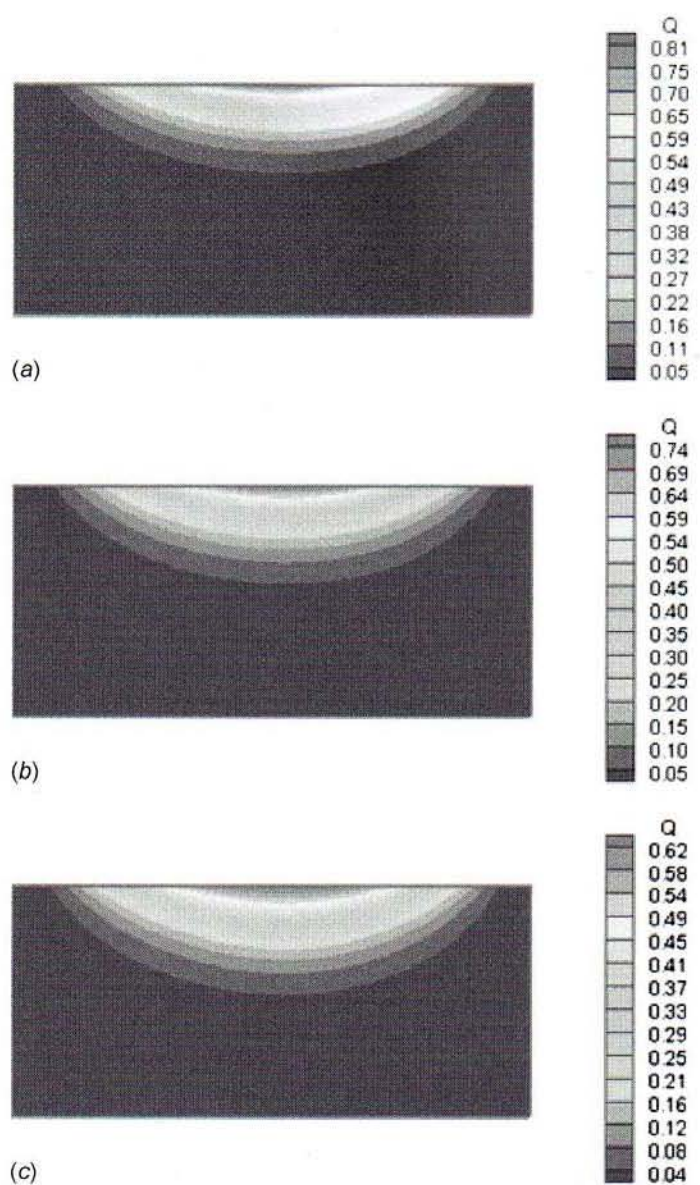


Fig. 16 Microwave power absorbed (MW/m^3) at various heating times (Case 4): (a) 20 s; (b) 40 s; (c) 60 s

except the reflected wave from the upper surface of the sample, are absorbed by the sample (Fig. 16). This phenomenon explains why the electric field and therefore the microwave power absorbed are the greatest at the surface exposed to incident microwaves and decay exponentially along the propagating direction with a very short wavelength, resulting in a thinner thermally stratified layer. In addition, the temperature distribution varies significantly from the maximum temperature to the minimum temperature in a short distance and, after $z > 25$ mm, the temperature distributions are almost unchanged within heating time of 20 s.

It is evident from the figure that there is only one peak appearing on the temperature distribution for this case. The maximum temperature within the sample is approximately 113°C at $t=60$ s.

For microwave heating of cement paste with a microwave frequency of 1.5 GHz (Case 5), the temperature profile within the sample (Fig. 17) displays a strong wavy behavior corresponding to the resonance of electric field (Fig. 10). This is because the electric field within the sample attenuates owing to energy absorption, and thereafter the absorbed energy is converted to the thermal energy, which increases the sample temperature. It is found that the temperatures decay slowly with a strong wavy behavior along the propagation direction following the absorption of microwave (Fig. 18).

Figures 19 and 20 show the predicted results and the experi-

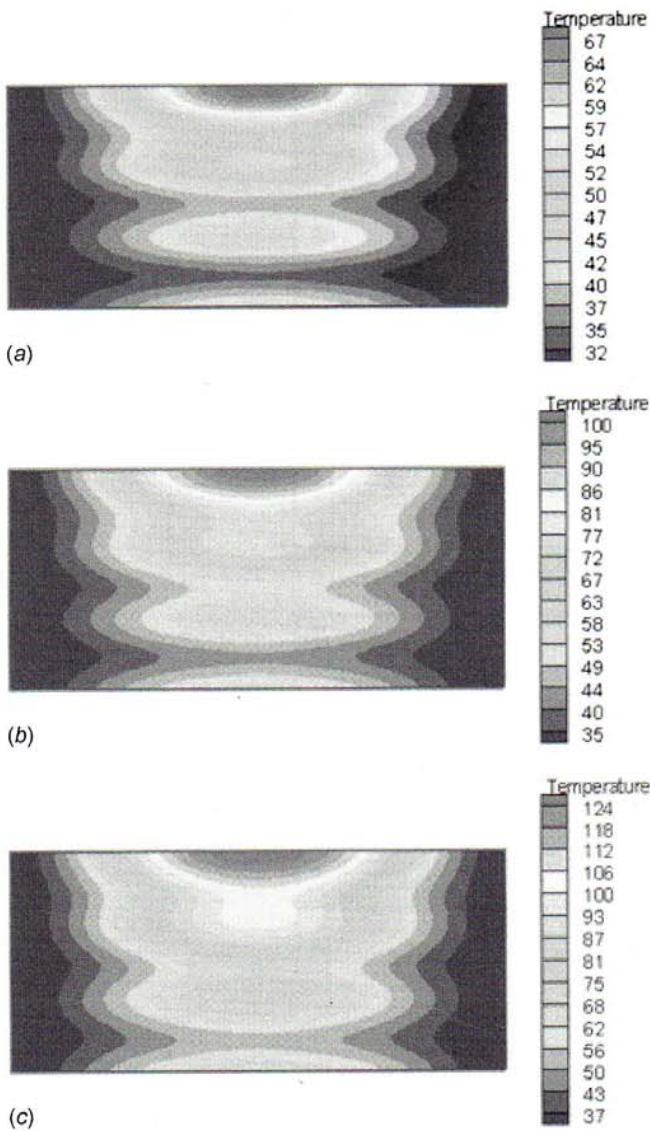


Fig. 17 Temperature distribution ($^{\circ}\text{C}$) at various heating times (Case 5): (a) 20 s; (b) 40 s; (c) 60 s

mental results (measured in symmetrical plane) of temperature distribution within the cement paste along with the horizontal axis of rectangular waveguide ($z=5$ mm) with different sample thicknesses (50 mm and 80 mm), which corresponds to the initial temperature of 25°C , microwave power level of 1000 W, and frequency of 2.45 GHz. The result shows the greatest temperature in the center of wood sample with the temperature decreasing toward the sidewalls of the sample. This phenomenon occurs because the TE_{10} field pattern displays a maximum electric field at the center of waveguide. It is shown that the predicted results agree well with the experimental result for the microwave heating of cement paste.

The prediction of temperature from mathematical model is compared with experimental data measured by infrared camera for microwave heating of cement paste, as shown in Fig. 21. It is shown that the predicted result agrees well with the experimental result for the microwave heating of cement paste particularly, the hot spot region. From the result, the capability of the mathematical model to correctly handle the field variations is shown. With further quantitative validation of the mathematical model, it is clear that the model can be used as an effective tool for investigating in detail this particular microwave heating of cement paste samples at a fundamental level.

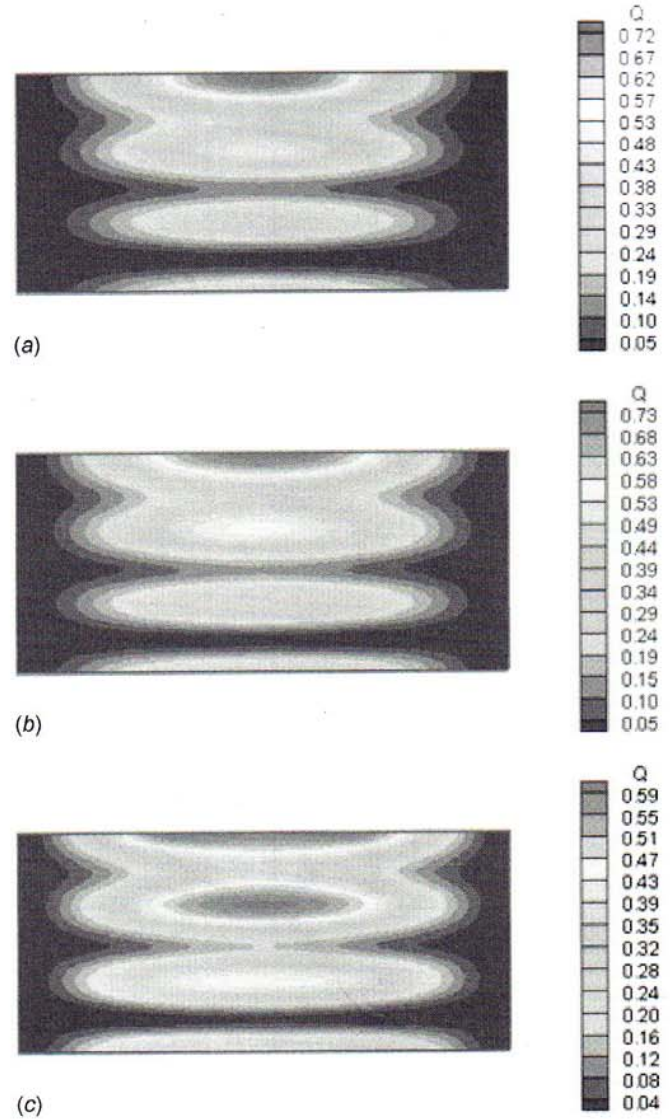


Fig. 18 Microwave power absorbed (MW/m^3) at various heating times (Case 5): (a) 20 s; (b) 40 s; (c) 60 s

7 Conclusions

The numerical analysis presented in this paper describes many important interactions within cement paste samples during microwave heating using a rectangular waveguide. The following paragraph summarizes the conclusions of this study.

- (1) A generalized mathematical model for microwave heating of cement paste is proposed. It is used successfully to describe the heating phenomena under various conditions.
- (2) The effects of irradiation times, working frequencies, and sample size on the microwave power absorbed and heating pattern that are developed within cement paste samples are clarified in detail. It can be concluded that the temperature distributions along the propagating wave show nonevidence of wavy behavior for Cases 3 and 4, which is inconsistent with what was exhibited for Cases 2 and 5. This result highlights that the working frequencies and sample size have significant effect on the heating characteristics. The simulated results for the temperature distributions within the cement paste samples rate are in agreement with experimental results. Figure 22 shows the generalized heating characteristics for Cases 2, 3, 4, and 5 for cement paste samples. The typical heating characteristics may be useful to provide guidance for optimal microwave processing of dielectric materials.

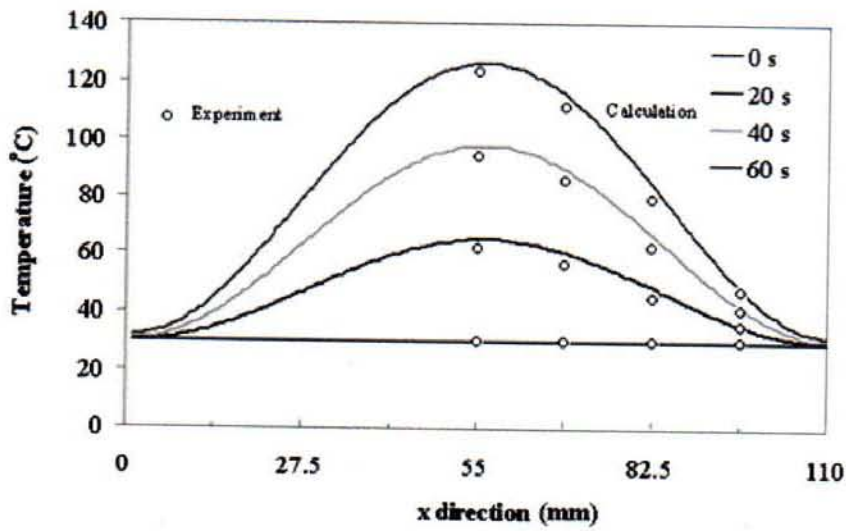


Fig. 19 Temperature distribution in cement paste along horizontal axis ($z = 50$ mm) ($P=1000$ W, $f=2.45$ GHz, size= 110 mm (x) \times 50 mm(z))

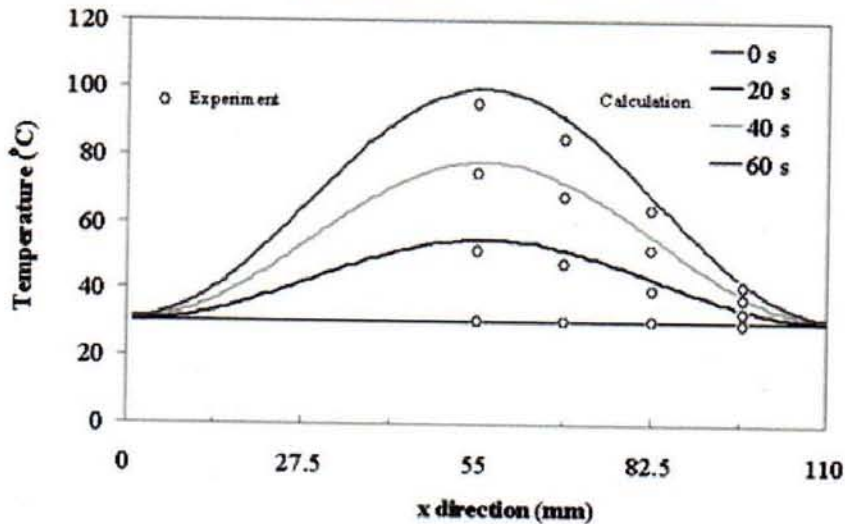


Fig. 20 Temperature distribution in cement paste along horizontal axis ($z = 50$ mm) ($P=1000$ W, $f=2.45$ GHz, size= 110 mm (x) \times 80 mm(z))

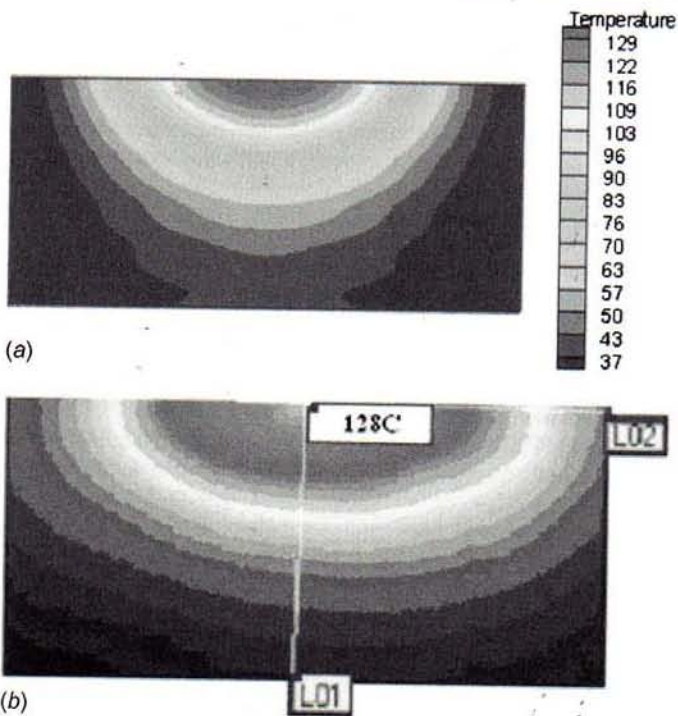


Fig. 21 The comparison of temperature distribution ($^{\circ}$ C) in wood sample: (a) simulated result and (b) experimental result

Acknowledgment

The authors are pleased to acknowledge Thailand Research Fund (TRF) for supporting this research work. The authors are also pleased to acknowledge Entech Associate Co., Ltd (Thailand) and Infra Tec GmbH (Germany) for providing thermographic measurement system.

Nomenclature

- A = area (m^2)
- B = magnetic flux density (Wb/m^2)
- C_p = specific heat capacity (J/kg K)
- D = electric flux density (C/m^2)
- E = electric field intensity (V/m)
- f = frequency of incident wave (Hz)
- H = magnetic field intensity (A/m)
- P = power (W)
- Q = local electromagnetic heat generation term (W/m^3)
- T = temperature ($^{\circ}$ C)
- t = time (s)
- $\tan \delta$ = loss tangent coefficient
- Z_H = wave impedance (Ω)
- Z_I = intrinsic impedance (Ω)









	(a) Case 2	(b) Case 3	(c) Case 4	(d) Case 5
Temperature Distribution				
Microwave Power Absorbed				
Conclusions	The optimal sample size and microwave frequency causes greater heating rates. A weak wavy behavior within the sample is formed	Heating pattern is not influenced by resonance. The wavy behavior within the sample is totally absent.	Heating pattern is not influenced by resonance and greater temperature takes place near the exposed surface. The wavy behavior within the sample is totally absent.	Heating pattern is influenced by resonance. The strong wavy behavior within the sample is formed.

Fig. 22 The heating characteristics for various heating conditions due to microwave energy for (a) case 2, (b) case 3, (c) case 4, (d) case 5. The darker shaded region represents the hot spot.

Greek Letters

- ε = permittivity (F/m)
- ϕ = porosity
- λ = wavelength (m)
- μ = magnetic permeability (H/m)
- ν = velocity of propagation (m/s)
- ρ = density (kg/m^3)
- σ = electric conductivity (S/m)
- ω = angular frequency (rad/s)

Subscripts

- a = air phase
- l = liquid phase
- p = solid phase
- r = relative
- x, y, z = coordinates
- 0 = free space, initial condition

References

- [1] Ayappa, K. G., Davis, H. T., Crapiste, G., Davis, E. A., and Gordon, J., 1991, "Microwave Heating: An Evaluation of Power," *Chem. Eng. Sci.*, **46**, pp. 1005–1016.
- [2] Ayappa, K. G., Davis, H. T., Davis, E. A., and Gordon, J., 1992, "Two-Dimensional Finite Element Analysis of Microwave Heating," *AIChE J.*, **38**, pp. 1577–1592.
- [3] Saltiel, C., and Datta, A., 1997, "Heat and Mass Transfer in Microwave Processing," *Adv. Heat Transfer*, **30**, pp. 1–94.
- [4] Tada, S., Echigo, R., Kuno, Y., and Yoshida, H., 1998, "Numerical Analysis of Electromagnetic Wave in Partially Loaded Microwave applicator," *Int. J. Heat Mass Transfer*, **41**, pp. 709–718.
- [5] Rattanadecho, P., Aoki, K., and Akahori, M., 2001, "A numerical and Experimental Study of Microwave Drying Using a Rectangular Wave Guide," *Drying Technol.*, **19**, pp. 2209–2234.
- [6] Rattanadecho, P., Aoki, K., and Akahori, M., 2002, "Influence of Irradiation Time, Particle Sizes and Initial Moisture Content During Microwave Drying of Multi-Layered Capillary Porous Materials," *ASME J. Heat Transfer*, **124**, pp. 151–161.
- [7] Rattanadecho, P., Aoki, K., and Akahori, M., 2002, "Experimental Validation of a Combined Electromagnetic and Thermal Model for a Microwave Heating of Multi-Layered Materials Using a Rectangular Wave Guide," *ASME J. Heat Transfer*, **124**(5), pp. 992–996.
- [8] Basak, T., 2003, "Analysis of Resonances During Microwave Thawing of Slabs," *Int. J. Heat Mass Transfer*, **46**, pp. 4279–4301.
- [9] Basak, T., 2004, "Role of Resonances on Microwave Heating of Oil-Water Emulsions," *AIChE J.*, **50**, pp. 2659–2675.
- [10] Akkari, E., Chevallier, S., and Boillereaux, L., 2005, "A 2D Non-Linear 'Grey-Box' Model Dedicated to Microwave Thawing: Theoretical and Experimental Investigation," *Comput. Chem. Eng.*, **30**(2), pp. 321–328.
- [11] Rattanadecho, P., Aoki, K., and Akahori, M., 2002, "A Numerical and Experimental Investigation of the Modeling of Microwave Heating for Liquid Using a Rectangular Wave Guide (Effect of Natural convection and Electrical Conductivity)," *J. Turbomach.*, **26**(3), pp. 449–472.
- [12] Watson, A., 1968, "Curing of Concrete," *Microwave Power Engineering*, E. C. Okress, ed., Academic, New York.
- [13] Delia, G. B., Lai, S., and Pinna, M., 1994, "Microwaves for the Hyper-Accelerated Curing of Concretes," *Betonwerk Fertigteil-Tech./Concrete Precasting Plant and Technology*, **60**(12), pp. 87–93.
- [14] Dongxu, L., and Xuequan, W., 1993, "A Study on the Application of Vacuum Microwave Composite Dewatering Technique in Concrete Engineering," *Cem. Concr. Res.*, **24**, pp. 159–164.
- [15] Hutchison, J. T., Chang, H. M., Jennings, H. M., and Brodwin, M. E., 1991, "Thermal Acceleration of Portland Cement Mortars With Microwave Energy," *Cem. Concr. Res.*, **21**, pp. 795–799.
- [16] Leung, C. K., and Pheeraphan, T., 1995, "Very High Early Strength of Microwave Cured Concrete," *Cem. Concr. Res.*, **25**(1), pp. 136–146.
- [17] Leung, C. K., and Peeraphan, T., 1995, "Microwave Curing of Portland Cement Concrete: Experimental Results and Feasibility for Practical Applications," *Constr. Build. Mater.*, **9**(2), 67–73.
- [18] Li, W., Ebadian, M. A., White, T. L., and Grubb, R. G., 1993, "Heat Transfer Within a Concrete Slab Applying the Microwave Decontamination Process," *ASME J. Heat Transfer*, **115**, pp. 42–50.
- [19] Mak, S. L., Sagoe-Crentsil, K. K., Taylor, A. H., and Ritchie, D., 1995, "Application of Microwave-Accelerated Processing in Cement and Concrete Technology," *Proceedings of 20th Conference on Our World in Concrete and Structures*, Vol. 15, C. T. Tan, ed., Otani, Singapore, Mar. 23–25, pp. 117–120.
- [20] Mak, S. L., Shapiro, O., and Son, T., 1998, "Accelerated Heating of Concrete With Microwave Curing," *Proceedings of the Fourth CANMET/ACI/JCI International Conference on Recent Advances in Concrete Technology*, Tokushima, Japan, Jun. 7–11, pp. 531–542.
- [21] Wu, X., Dong, L., and Tang, M., 1987, "Microwave Curing Technique in Concrete Manufacture," *Cem. Concr. Res.*, **17**, pp. 205–210.
- [22] Perre, P., and Turner, W., 1997, "Microwave Drying of Softwood in an Oversized Waveguide," *AIChE J.*, **43**, pp. 2579–2595.
- [23] Zhao, H., and Turner, I. W., 2000, "The Use of a Coupled Computational Model for Studying the Microwave Heating of Wood," *J. Turbomach.*, **24**, pp. 183–197.
- [24] Rattanadecho, P., 2006, "The Simulation of Microwave Heating of Wood Using a Rectangular Wave Guide (Influence of Frequency and Sample Size)," *Chem. Eng. Sci.*, **61**(14), pp. 4571–4581.
- [25] American Society for Testing and Materials, 2006, *Annual Book of ASTM Standard Vol. 4, No. 02*, Philadelphia PA.
- [26] Von Hippel, A. R., 1954, *Dielectric Materials and Applications*, MIT, Boston.
- [27] Mak, S. L., Banks, R. W., Ritchie, D. J., and Shapiro, G., 2002, "Advances in Microwave Curing of Concrete," *Fourth World Congress on Microwave & Radio Frequency Applications*, Sydney, Australia, Sept. 22–26.
- [28] Rattanadecho, P., 2004, "The Theoretical and Experimental Investigation of Microwave Thawing of Frozen Layer Using Microwave Oven (Effects of Layered Configurations and Layered Thickness)," *Int. J. Heat Mass Transfer*, **47**, pp. 937–945.
- [29] Rattanadecho, P., Suwannapum, N., Chatveera, B., Atong, D., and Makul, N., 2008, "Development of Compressive Strength of Cement, Paste Under Accelerated Curing by Using a Continuous Microwave Belt Drier," *Mater. Sci. Eng.-A*, **472**, pp. 299–307.